Electronic Supplementary Material (ESI) for Nanoscale.

Metal-Organic Frameworks/Polydopamine Synergistic Interface Enhancement of Carbon Fiber/Phenolic Composites with Promoting Mechanical and Tribological Performances

Shanshan Ma, Hejun Li*, Chang Li, Haochen Tian, Meixia Tao, Jie Fei*, Lehua Qi

State Key Laboratory of Solidification Processing, Shaanxi Key Laboratory of Fiber Reinforced Light Composite Materials, Northwestern Polytechnical University, Xi'an, 710072, China

** Corresponding author. Tel: +8613609262816. E-mail: lihejun@nwpu.edu.cn (Hejun Li)*

Tel: +8613488142894. E-mail: feijiecc@nwpu.edu.cn (Jie Fei)

1. SEM analyses of functionalized CFs

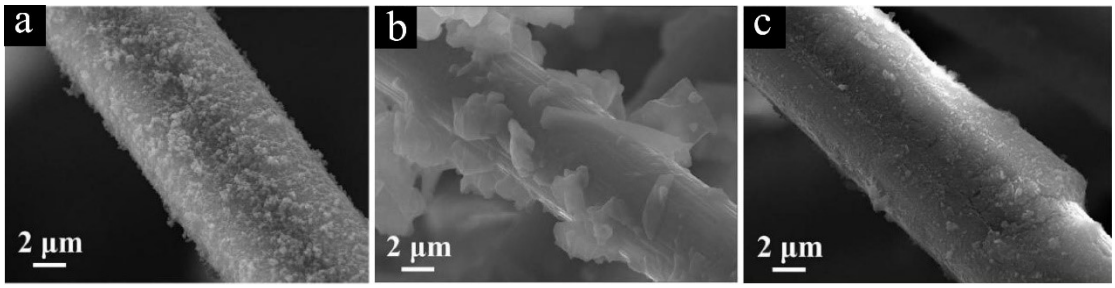

Figure S1. (a) ZIF-8-CF, (b) MOF-5-CF and (c) UiO-66-$(COOH)_2$-CF.

Figure S1 showed the surface morphology of ZIF-8-CF, MOF-5-CF and UiO-66-$(COOH)_2$-CF. Numerous ZIF-8 nanoparticles in situ uniformly surface of PDA-CF and tightly attached to the fibers (Figure S1a). As shown in Figure S1b, the MOF-5 crystals evenly distributed and grew around the PDA-CF. Furthermore, Figure S1c indicated the formation of a dense UiO-66-$(COOH)_2$ crystal layer on the surface of carbon fibers. Therefore, the three kinds of crystals were not simply physically deposited on the fiber surface, but form a certain chemical interaction with fibers. This chemical bonding could effectively prevent the crystals falling off under working conditions.

2. XRD, FTIR, XPS and Raman analyses of modified CFs

The crystallinity of pristine CF, PDA-CF, ZIF-8-CF, MOF-5-CF, UiO-66-$(COOH)_2$-CF and multiscale MOFs was determined by the X-ray diffraction. As shown in Figure 4a, various fibers all displayed a broad peak located at $2\theta = 25.5°$, which was assigned to the typical graphitic stacking structure of carbon fibers[1]. The ZIF-8-CF exhibited several new characteristic peaks[2] located at 2θ = 7.4°(011), 10.5°(002), 12.7°(112), 14.7°(022), 16.4°(013), and 18.1°(222), consistent with the ZIF-8 crystal in Figure S2b. The diffraction peaks located at 2θ = 6.8°(200), 9.8°(220), and 15.5°(400) were attributed to the MOF-5 crystal as reported in the literature[3]. The above typical peaks could also be observed in MOF-5-CF in Figure 4a. The XRD pattern of UiO-66-$(COOH)_2$ crystal showed two sharp characteristic peaks at 2θ =7.4°(111) and 8.5°(002) as reported by Hua and his coworkers[4]. These typical diffraction peaks could also be found in UiO-66-$(COOH)_2$-CF in Figure 4a. The new and sharp characteristic peaks on the MOFs-CF were absent in pristine CFs, suggesting the immobilization of multiscale MOFs crystals on the surface of carbon fibers.

FTIR spectra of pristine CF, PDA-CF, ZIF-8-CF, MOF-5-CF, UiO-66-$(COOH)_2$-CF were observed in Figure 4b. Compared with pristine CF, the PDA-CF displayed a new weak absorption band at 3422 cm^{-1}, which could be assigned to O-H stretching vibration and N-H stretching vibration. The result was consistent with Chen and his coworkers[5]. The Zn-O characteristic stretching vibrations[6] was characterized by 440 cm^{-1}. The ZIF-8-CF showed the characteristic absorption peaks at 1582 cm^{-1}, 3121 cm^{-1} and 2910 cm^{-1}, which could be ascribed to the C=N stretching in imidazole ring and the aromatic and aliphatic C-H stretch vibrations[7], respectively. Furthermore, the typical FTIR spectra of ester function should indicate three strong characteristic absorption peaks about 1725 cm^{-1} belonged to C=O and 1160 cm^{-1}, 1310 cm^{-1} belonged to C-O-C. Because of the conjugative effect of benzene, the absorption peak of -C=O- shifted to around 1670 cm^{-1} in MOF-5-CF and UiO-66-$(COOH)_2$-CF[3, 8]. The absorption peaks of 1147 cm^{-1} and 1303 cm^{-1} in MOF-5-CF and UiO-66-$(COOH)_2$-CF were associated with the symmetric and asymmetric -C-O-C- stretching band of ester function with benzene[9].

Moreover, the most interesting Zr-O symmetric and asymmetric stretching vibrations[10] at 622 and 560 cm^{-1} were observed in Figure 4b. The above results were consistent with the results of SEM and XRD, further confirming the in situ growth of multiscale MOFs on the CFs surface.

The surface chemical performances of various CFs including pristine CF, PDA-CF, ZIF-8-CF, MOF-5-CF, UiO-66-$(COOH)_2$-CF were analyzed by X-ray photoelectron spectroscopy (Figure 4c-f). From the wide spectra, ZIF-8-CF, MOF-5-CF and UiO-66-$(COOH)_2$-CF indicated the typical Zn 2p and Zr 3d peaks, which were absent from pristine CF and PDA-CF in Figure 4c. Moreover, the detailed XPS analysis could be observed in Figure 4d-f, suggesting the formation of homogeneous MOFs layer on the PDA-CF surface. The ZIF-8-CF and MOF-5-CF both exhibited a Zn 2p fitting peak, conforming the results reported by Shah and his coworkers[11, 12]. Furthermore, the UiO-66-$(COOH)_2$-CF also showed a typical Zr 3d peak located at 183.0 and 180.5 eV as reported in the literature[10]. The XPS results further conformed the successful growth and immobilization of MOFs crystals on the fibers surface.

The molecular structure of pristine CF, PDA-CF, ZIF-8-CF, MOF-5-CF and UiO-66-$(COOH)_2$-CF was analyzed by the Raman spectra and related results were shown in Figure 5c. Two strong peaks, D band (1350 cm^{-1}) and G band (1600 cm^{-1}) could be obviously observed in the recorded Raman spectrum, indicating that a series of chemical treatments did not affect the structural integrity of carbon fibers. The intensity ratio I_D/I_G was 1.05 for pristine CF, while those of PDA-CF, ZIF-8-CF, MOF-5-CF and UiO-66-$(COOH)_2$-CF were 1.06, 1.24, 1.13 and 1.07, respectively. The value (R) of I_D/I_G is related to the degree of graphitization and disorder. The slight increasement in the intensity ratio value of PDA-CF could be attributed to the introduction of certain structure defects during preliminary ultrasonic treatment. Moreover, owing to the MOFs crystals with defective structures, the value of R tends to increase compared to the pristine carbon fibers, meaning the rising of disorder carbon atom number on the CFs surface.

3. Dynamic friction coefficient of samples under different working conditions

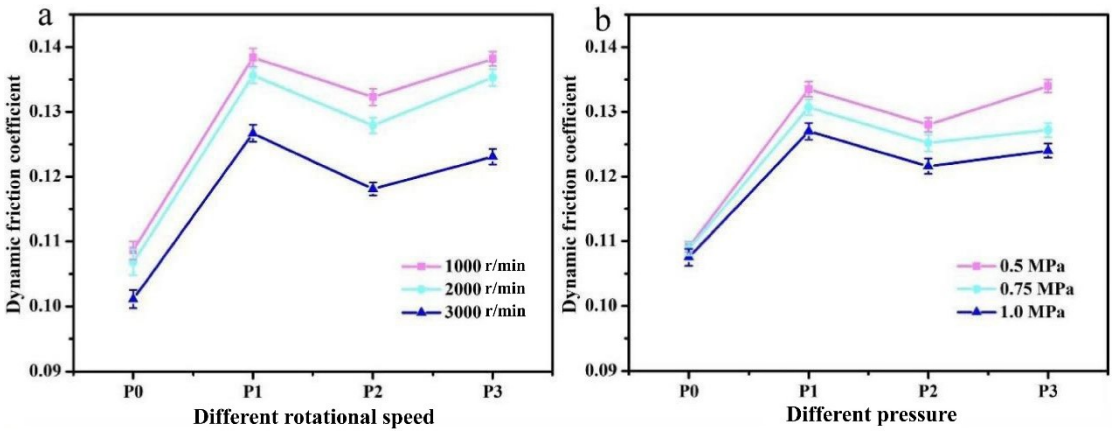

Figure S2. The effect of (a) different rotational speed and (b) pressure on the dynamic friction coefficient of the composites.

The effects of brake pressure and rotational speed on the dynamic friction coefficient of the composites were investigated as shown in Figure S2a-b. Whether the increase in the working rotational speed or the brake pressure, it would lead to the decrease of the dynamic friction coefficient. With the rotational speed changes from 1000 to 3000 r/min, the temperature of the interface went up significantly during this process, causing the composites to thermal degrade and the friction coefficient to decrease. Moreover, under higher brake pressure, the engagement time of the mechanical interlock between the materials and friction pairs decreased. In the meanwhile, a large amount of lubricating oil was squeezed onto the friction surface to form a thicker oil film, thereby covering the protrusions and reducing mechanical contact. In addition, compared with the control sample (P0), the modified samples, especially P1, could work well under the conditions of heavy loading and high speed.

References

[1] Huang, Y.; Young, R. J. Effect of fiber microstructure upon the modulus of PAN- and pitch-based carbon fibres. *Carbon* **1995**, *33* (2), 97-107.

[2] He, M.; Yao, J.; Liu, Q.; Wang, K.; Chen, F.; Wang, H. Facile synthesis of zeolitic imidazolate framework-8 from a concentrated aqueous solution. *Micropor. Mesopor. Mat*. **2014**, *184*, 55-60.

[3] Yang, Q.; Zhang, M.; Song, S.; Yang, B. Surface modification of PCC filled cellulose paper by MOF-5 ($Zn_3(BDC)_2$) metal–organic frameworks for use as soft gas adsorption composite materials. *Cellulose* **2017**, *24* (7), 3051-3060.

[4] Hua, W.; Zhang, T.; Wang, M.; Zhu, Y.; Wang, X. Hierarchically structural PAN/UiO-66-$(COOH)_2$ nanofibrous membranes for effective recovery of Terbium(III) and Europium(III) ions and their photoluminescence performances. *Chem. Eng. J.* **2019**, *370*, 729-741.

[5] Yuan, H.; Wang, C.; Zhang, S.; Lin, X. Effect of surface modification on carbon fiber and its reinforced phenolic matrix composite. *Appl. Surf. Sci*. **2012**, *259*, 288-293.

[6] Bustamante, E. L.; Fernández, J. L.; Zamaro, J. M. Influence of the solvent in the synthesis of zeolitic imidazolate framework-8 (ZIF-8) nanocrystals at room temperature. *J. Colloid Interf. Sci.* **2014**, *424*, 37-43.

[7] Hu, Y.; Kazemian, H.; Rohani, S.; Huang, Y.; Song, Y. In situ high pressure study of ZIF-8 by FTIR spectroscopy. *Chem. Commun.* **2011**, *47* (47), 12694-12696.

[8] Park, K.; Ni, Z.; Cote, A.; Choi, J.; Huang, R.; Uribe-Romo, F.; Chae, H.; O'Keeffe, M.; Yaghi, O. Exceptional chemical and thermal stability of zeolitic imidazolate frameworks. *P. Nati. Acad. Sci. USA* **2018**, *103* (27), 10186-10191.

[9] Mirkovic, I.; Lei, L.; Ljubic, D.; Zhu, S. Crystal Growth of Metal-Organic Framework-5 around Cellulose-Based Fibers Having a Necklace Morphology. *ACS Omega* **2019**, *4* (1), 169-175.

[10] Yang, X.; Jiang, X.; Huang, Y.; Guo, Z.; Shao, L. Building nanoporous metal-organic frameworks “armor” on fibers for high-performance composite materials, *ACS Appl. Mater. Inter.* **2017**, *9*, 5590-5599.

[11] Ubaidullah, M.; Al-Enizi, A. M.; Shaikh, S.; Ghanem, M. A.; Mane, R. S. Waste PET plastic derived ZnO@NMC nanocomposite via MOF-5 construction for hydrogen and oxygen evolution reactions. *J. King Saud Univ. Sci.* **2020**, *32* (4), 2397-2405.

[12] Shah, M.; Kwon, H. T.; Tran, V.; Sachdeva, S.; Jeong, H.-K. One step in situ synthesis of supported zeolitic imidazolate framework ZIF-8 membranes: Role of sodium formate. *Micropor. Mesopor. Mat*. **2013**, *165*, 63-69.